Homogeneity Range, Hole Concentration, and Electrical Properties of the $Bi_2Sr_{3-x}Ca_xCu_2O_{8+y}$ ($1 \leqq x \leqq 2$) Superconductors

P. Ghigna, G. Chiodelli, U. Anselmi-Tamburini, G. Spinolo, and G. Flor

Department of Physical Chemistry and C.S.T.E./CNR, University of Pavia, Pavia, Italy

Z. Naturforsch. **48a**, 1214–1218 (1993); received October 26, 1993

The homogeneity range of Bi–Sr–Ca–Cu oxides with two-layers ("2212") structure has been investigated with X-ray powder diffraction and electron microprobe determination on materials with nominal $Bi_2Sr_{3-x}Ca_xCu_2O_{8+y}$ ($x = 1 \div 2$ in 0.1 steps) composition and being prepared at two different oxygen partial pressures. The results show Bi over-stoichiometry and a wide range of Sr/Ca substitution.

DC resistivity measurements indicate that the hole concentration is controlled by both oxygen non-stoichiometry and cation molecularity. It is shown that a single phenomenological relation between hole concentration and electrical properties can explain in a consistent way the complex behaviour of the whole set of materials with different oxygen non-stoichiometry and cation molecularity.

Key words: $Bi_2Sr_2CaCu_2O_8$; Superconductors; Oxygen non-stoichiometry; Cation molecularity.

1. Introduction

The family of oxide superconductors usually written as $Bi_2Sr_2Ca_{n-1}Cu_nO_{4+2n}$ ($n = 1$, 2, or 3) [1] shows a broad range of structural, chemical and physical properties. Three crystal structures with superconducting properties have been described for these materials: they are referred to, as the one-layer (L1, in the following), two-layers (L2), and three-layers (L3) structure because they correspond to different stacking sequences of the same building blocks. Formerly, a strict relation was believed to exist between each phase and the cation molecularity ($n = 1$, 2, or 3) of the family. It has later become clear that these crystal structures actually describe solid solutions with well measurable composition ranges, and that a family member may even fall outside the single-phase stability field of the corresponding structure [2–9]. Sr/Ca substitutional defects have been mainly investigated in this regard, but there is now general agreement that some amount of Bi occupies alkali earth sites.

On the other side, the superconducting properties of these materials are usually related with the electronic holes [h˙], that can be produced by quenching the oxygen over-stoichiometry obtained with high-temperature treatments under different oxygen partial pressures [10–14]. However, a strong influence between oxygen non-stoichiometry and cation molecularity should be expected on the basis of very general considerations about defect equilibria.

In this paper we provide experimental arguments showing the influence of cation molecularity and oxygen non-stoichiometry on hole concentration [h˙] and superconductivity of two-layers structure solutions by investigating the homogeneity range and electrical properties of a series of materials with *nominal* compositions described by $Bi_2Sr_{3-x}Ca_xCu_2O_{8+y}$ ($1 \leqq x \leqq 2$).

Reprint requests to Prof. G. Flor, Department of Physical Chemistry, viale Taramelli, 16, I-27100 Pavia (Italy).

2. Experimental

2.1. Materials

The starting materials Bi_2O_3, CuO, $CaCO_3$ and $SrCO_3$ (Aldrich 99.99%) were used as supplied. Appropriate amounts of the starting powders were mixed in acetone under vigorous stirring, dried, uniaxially pressed into pellets, and allowed to react at 1100 K under pure oxygen at 1 atm for a total time of 144 hours with one intermediate cooling step after 96 hours for grinding and re-pelletization. The starting (*nominal*) compositions of these materials are described by the general formula $Bi_2Sr_{3-x}Ca_xCu_2O_{8+y}$ with $x = 1$ to 2 at 0.1 steps.

A second series of materials was prepared by further heating each sample of the first series at 1020 K for 48 hours under 10^{-3} atm oxygen partial pressure.

0932-0784 / 93 / 1200-1214 $ 01.30/0. – Please order a reprint rather than making your own copy.

2.2. Instruments and Methods

Four-electrodes dc resistivity measurements were performed at $10\ K \leqq T \leqq 300\ K$ using a Solartron 1286 Electrochemical Interface and an LTC 60 temperature controller driving a Leybold ROK 19 cryostat. Using IEEE 488 interfaces, both devices were connected to a personal computer for sampling ϱ vs. T curves at 10 s intervals with a cooling rate of $5 \cdot 10^{-3}\ K\,s^{-1}$.

X-ray powder diffraction patterns were taken with a Philips 1710 diffractometer equipped with a copper anode (λ for K $\bar{\alpha}$ radiation = 0.15418 nm), graphite monochromator on the diffracted beam, and proportional counter, operated at 40 KV and 35 mA. The lattice dimensions were obtained with a programme [15] minimising the squared differences between calculated and experimental Q values ($Q_i = 4 \sin^2 \vartheta_i / \lambda^2$, ϑ_i = diffraction angle) with weights proportional to $[\sin(2\vartheta_i)]^{-2}$.

A Zeiss Axioplan and a Jeol JXA-840A equipped with wavelength dispersive detector were used, respectively, for optical and both electronic microscopy (SEM) and electron probe microanalysis (EMPA). The samples were prepared by inclusion in epoxy resin (Buehler) and polishing to optical flatness. For EMPA, the samples were covered with graphite. Bi and Cu were analysed with a LiF crystal using M and K radiations, respectively; Ca with a PET crystal and K radiation, Sr with a TAP crystal and L radiation, and the instrument was operated at 20 nA beam intensity and a 5 μm^2 spot. The standard materials for elemental analysis were polycrystalline sintered Bi_2O_3, SrF_2 (Aldrich 99.99%), and CaF_2 (Aldrich 99.9%) single crystals, and polycrystalline Cu metal (Jeol 99.9%). The standard deviations of the analytical determinations were always below 0.5%.

3. Results

The homogeneity range of the L2 phase was investigated by coupled X-ray powder Diffraction (XRPD) and Electron Microprobe Analysis (EMPA).

Figure 1 shows an XRPD pattern of a materials with $x = 1.5$. An inspection of the XRPD patterns of the whole series of the samples before and after heat treatment at $T = 1020\ K$ and $P(O_2) = 10^{-3}$ atm showed that:

- most samples are polyphasic, but in all samples L2 is the majority phase;

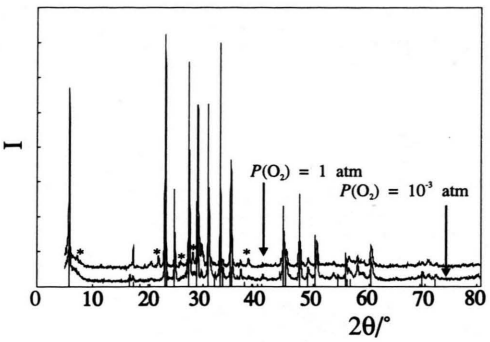

Fig. 1. X-ray patterns of a sample with nominal composition $Bi_2Sr_{1.5}Ca_{1.5}Cu_2O_{8+y}$, produced at $P(O_2) = 1$ atm (top pattern) and after heat treatment at $P(O_2) = 10^{-3}$ atm (bottom pattern). The vertical bars indicate the peaks of the L2 phase; the asterisks mark the most important impurity peaks.

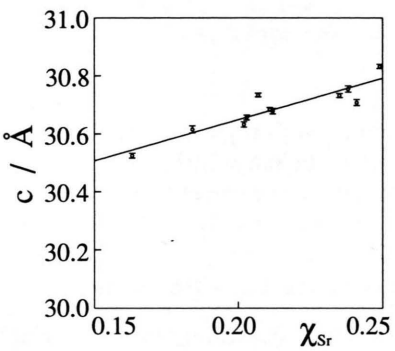

Fig. 2. Lattice dimension c of L2 structure as a function of the effective Sr content (χ_{Sr}).

- the lattice dimension c of L2 rises as the Sr content rises (Figure 2);
- in samples produced under 1 atm O_2 the largest impurity is L1;
- in samples produced under 10^{-3} atm O_2 the amount of L1 is generally lower and vanishes in the $1.2 \leqq x \leqq 1.7$ range; these samples also contain $(Sr, Ca)_{24}Cu_{14}O_{41}$ and $(Sr, Ca)_2CuO_3$ impurities at high and low Sr content, respectively.

The relative amounts of the spurious phases, as inferred by XRPD, is shown in Figure 3.

For the EMPA determinations, seemingly single-phase areas were selected by careful inspection of the samples under SEM. The results show that:

- within the experimental errors, the heat treatment at 10^{-3} atm O_2 does not change the cation molecularity of the L2 phase;

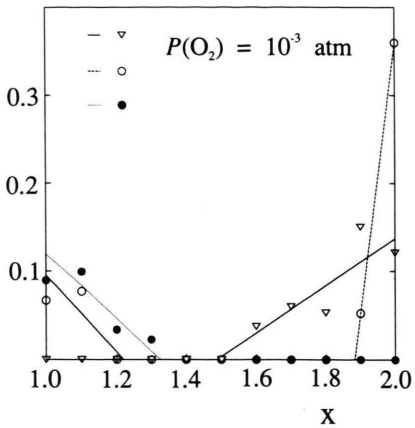

Fig. 3. Phase impurities of the investigated materials as a function of the nominal Sr content (x in $Bi_2Sr_{3-x}Ca_xCu_2O_{8+y}$). The ordinates are ratios of X-ray powder diffraction intensities. Triangles: (111)-Ca_2CuO_3 to (200)-L2; open circles: (113)-L1 to (115)-L2; filled circles: (400)-$Sr_{14}Cu_{24}O_{41}$ to (115)-L2.

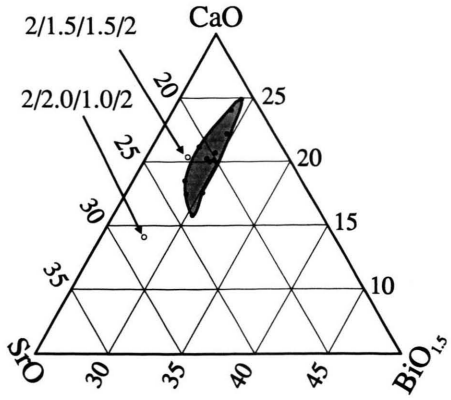

Fig. 4. Homogeneity range of the L2 phase. The filled circles indicate experimental determinations. Empty circles correspond to indicated ratios Bi/Sr/Ca/Cu.

- Bi is always in excess with respect to "2212" molecularity, and varies in the range $1.04 \leqq Bi/Cu \leqq 1.27$;
- the total amount of alkali earth cations (Sr + Ca) is generally lower than expected from "2212" molecularity: $2.91 \leqq (Sr + Ca) \leqq 3$;
- the Sr/Ca ratio is in the $1.47 \div 0.64$ range.

To make clear the deviation from nominal compositions (above that described by x in $Bi_2Sr_{3-x}Ca_xCu_2O_{8+y}$), the true cation molecularities obtained by EMPA determinations will be indicated in the following as ratios (χ_j) of the amounts of the different cations ($j \in I = \{Ca, Sr, Cu, Bi\}$):

$$\chi_j = \frac{n(j)}{\sum_{i \in I} n(i)}.$$

The whole set of XRPD and EMPA results is in qualitative agreement with previous data [16–19]. For easier comparison, Figure 4 shows the homogeneity range of the L2 phase in a plane parallel to the Ca–Sr–Bi basis using a representation similar to that of Golden et al. [16] and Holesinger et al. [18]: χ_{Ca}, χ_{Sr} and χ_{Bi} are here normalized to constant $\chi_{Cu} = 0.3$. Quantitatively, our data indicate a lower Bi content (i.e. a lower Bi excess with respect to "2212") than the result of Golden et al. [16]. With respect to Holesinger et al. [18], the present results show a lower Sr/Ca ratio but a very close Bi content. These discrepancies may well be explained making reference to the presence of the L1 phase found by Golden et al. [16]. Moreover, it is worth noting that Holesinger et al. [18] prepared their samples at higher temperatures, and that higher preparation temperatures correspond to higher Sr/Ca ratios (see Majevski et al. [19]).

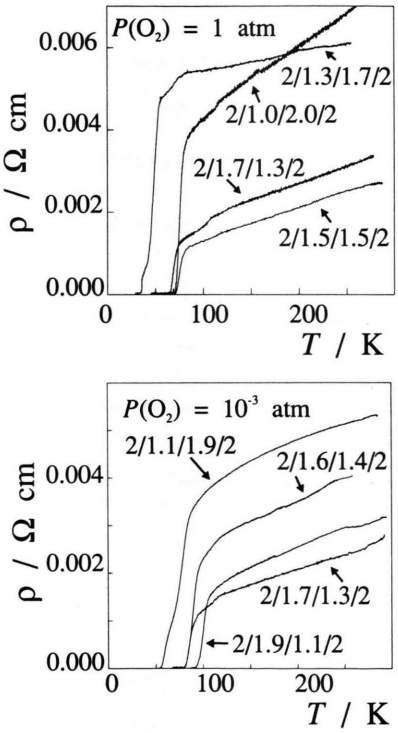

Fig. 5. Resistivity (ϱ) of samples with different nominal compositions prepared at $P(O_2) = 1$ atm (a) and $P(O_2) = 10^{-3}$ atm (b)

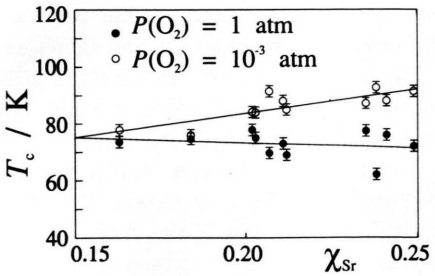

Fig. 6. Critical temperature (onset) as a function of the effective Sr content (χ_{Sr}).

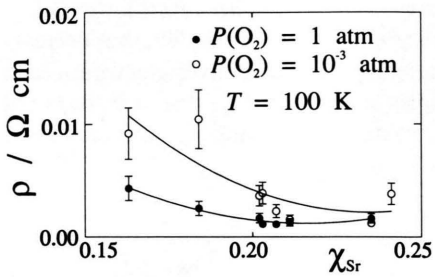

Fig. 7. Resistivity at $T = 100$ K as a function of the effective Sr content (χ_{Sr}).

Figures 5a and 5b show the resistivity (ϱ) vs. temperature (T) plots of samples produced at 1 atm O_2 and 10^{-3} atm O_2, respectively. It is apparent from the figures that the superconducting transition is sharp when the nominal Sr content $(3-x)$ is above 1.7. At lower Sr contents, the transition becomes diffuse and happens at lower critical temperatures, the ϱ values are 3–4 times higher than those of the other samples, and the ϱ vs. T curves show a complex shape in the $40 \leqq T \leqq 60$ K range. This is clearly due to the presence of another superconducting phase, that has been identified by XRPD and EMPA as a Ca-rich L1 phase and can be provisionally written as $Bi_2(Sr_{1-x}Ca_x)_2CuO_y$.

Figure 6 reports the (onset) T_c at different χ_{Sr} for both the low-$P(O_2)$ and high-$P(O_2)$ series of samples. It is worth noting here the different values and signs of the slopes for the two series, as well as the seemingly converging trends towards a single value at the low χ_{Sr} side. Finally, Fig. 7 shows how the resistivity (at the selected temperature of 100 K) changes with χ_{Sr}.

4. Discussion

There is general agreement about the very important influence of holes localised in the CuO_2 planes on the superconducting properties of CuO-based materials having perovskite-related structures. Accordingly, a precise knowledge of *both* (cation) molecularity *and* (oxygen) stoichiometry is an obvious prerequisite to the understanding of relations between hole concentration and superconductivity.

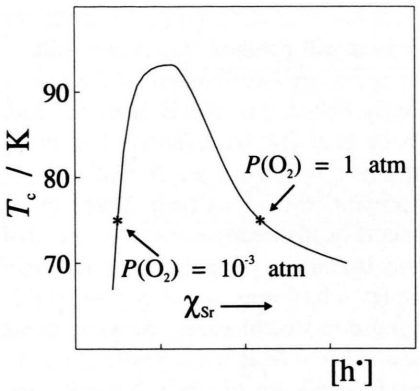

Fig. 8. Phenomenological relation between hole concentration and critical temperature, redrawn with modifications after [18]. The stars indicate the low-χ_{Sr} samples that show almost the same T_c after heat treatments at $P(O_2) = 1$ atm and $P(O_2) = 10^{-3}$ atm. The arrow indicates the effect on electrical properties of changing hole concentration by rising Sr content.

The superconducting phase here discussed is characterised by a significant oxygen over-stoichiometry in a wide $P(O_2)$ range [10–14]. For that reason it has usually been assumed (implicitly) that the hole concentration [h•] can be directly evaluated from a measurement of oxygen non-stoichiometry, because of the defect reaction

$$1/2\,O_2 = O_i'' + 2h^\bullet. \tag{1}$$

By showing the large molecularity range of *differently charged* cations, the present results indicate that the cation molecularity must be carefully considered, in addition to the oxygen non-stoichiometry, when evaluating [h•]. Taking into account that excess Bi occupies Sr sites [5], it is possible to write the following defect equation:

$$Bi + Sr_{Sr} + h^\bullet = Bi_{Sr}^\bullet + Sr, \tag{2}$$

which shows that one hole is destroyed when one $Bi_{Sr}^\bullet$ substitutional defect is formed. Since the L2 phase always contains Bi excess ($Bi_{Sr}^\bullet$ defects), its hole concentration is always lower than inferred by measuring the oxygen content. It is worth noting that most of the conclusions below do not depend on the particular

nature of the defect involved in the equilibrium (2): for instance, $Bi_{Ca}^{\cdot}$ defects will produce the same result.

The critical temperature has frequently been correlated with $[h^{\cdot}]$, and a bell-shaped plot is then obtained. For instance, Pham et al. [14] have shown that the T_c maximum occurs at $y = 0.12$ for $Bi_2Sr_2CaCu_2O_{8+y}$ materials. The present results can be analysed in an analogous manner (Fig. 8) directly using $[h^{\cdot}]$ instead of their y coordinate. Because of the polyphasic nature of some of the samples, it has been considered unreliable to perform oxygen non-stoichiometry measurements on these materials. Therefore, it is not possible here to indicate a precise $[h^{\cdot}]$ scale for Figure 8. Nevertheless, a sound conclusion can be drawn by simply considering how T_c changes by changing the Sr and O content of the samples.

Let us start from the remark (see again Fig. 6) that the samples with the lowest *effective* Sr content (χ_{Sr}) show practically the same T_c after heat treatment at $P(O_2) = 1$ and $P(O_2) = 10^{-3}$ atm. Therefore, they can in Fig. 8 be placed at the same ordinate on either side of the bell-shaped curve (in particular: the low-$P(O_2)$ sample on the left branch, the high-$P(O_2)$ sample on the right branch). Going now to higher Sr contents, the $Bi_{Sr}^{\cdot}$ defect concentration decreases, thus producing a larger $[h^{\cdot}]$ because of reaction (2), and therefore a rightwards shift along the curve. The result is that low-$P(O_2)$ samples show higher T_c values at higher Sr content, whereas the T_c of high-$P(O_2)$ samples decreases as the Sr content rises. Note, however, that the latter trend is expected to be less marked than the former one because of the shape of the curve.

An analogous conclusion can be drawn by inspecting Figure 7. Indeed, all the samples obtained by heat treatment at 1020 K and $P(O_2) = 10^{-3}$ atm show higher ϱ values than those having the same χ_{Sr} but produced under 1 atm oxygen, because a lower $P(O_2)$ shifts the equilibrium (1) towards the left, thus decreasing $[h^{\cdot}]$ and therefore rising ϱ. Conversely, within each series of samples at fixed $P(O_2)$, the substitutional defect $Bi_{Sr}^{\cdot}$ decreases by increasing χ_{Sr}, thus increasing $[h^{\cdot}]$ and reducing ϱ.

Acknowledgements

This work has been partially supported by the Ministry of University of Scientific and Technological Research of the Italian Government (MURST-40%).

[1] H. Maeda, Y. Tanaka, M. Fukutomi, and J. Asano, Japan J. Appl. Phys. **27,** 120 (1988).
[2] A. M. Chippindale, S. J. Hibble, U. J. Hrijac, L. Cowey, D. M. S. Bapjuley, P. Day, and A. K. Cheetham, Physica **C 152,** 154 (1988).
[3] H. W. Zandbergen, W. A. Graen, F. C. Mijlhott, G. van Tandeloo, and S. Amelink, Physica **C 156,** 325 (1988).
[4] G. S. Graden, E. M. Gyorgy, P. K. Gallegher, H. M. O'Bryan, D. W. Johnson, S. Sunshine, S. M. Zahurak, S. Jin, and R. C. Shervood, Phys. Rev. **B 38,** 757 (1988).
[5] A. K. Cheetham, A. M. Chippindale, S. J. Hibble, and C. J. Woodley, J. Phase Transitions **19,** 223 (1989).
[6] A. K. Cheetham, A. M. Chippindale, and S. J. Hibble, Nature London **33,** 21 (1988).
[7] A. W. Sleight, Science **242,** 1519 (1988).
[8] Y. Gao, P. Lee, P. Coppens, M. A. Subramanian, and A. W. Sleight, Science **241,** 954 (1988).
[9] H. Tokagi, H. Eisaki, S. Uchida, A. Maeda, S. Jajima, K. Uchinokura, and S. Tanaka, Nature London **332,** 236 (1988).
[10] J. E. Hirsch and F. Marsiglio, Phys. Lett. **A 140,** 122 (1989).
[11] W. A. Groen, D. M. De Leeuw, and L. F. Feiner, Physica **C 165,** 55 (1990).
[12] Y. Idemoto, S. Fujiwara, and K. Fueki, Physica **C 176,** 325 (1991).
[13] M. R. Presland, J. L. Tallon, R. G. Buckley, R. S. Liv, and N. E. Flower, Physica **C 176,** 95 (1991).
[14] A. Q. Pham, M. Hervieu, A. Maigan, C. Michel, J. Provost, and B. Raveau, Physica **C 194,** 243 (1992).
[15] U. Anselmi Tamburini and G. Spinolo, J. Appl. Cryst. **26,** 5 (1993).
[16] J. S. Golden, T. E. Bloomer, F. R. Lange, A. M. Jegadaes, E. Vaidya, and A. K. Cheetham, J. Amer. Ceram. Soc. **74,** 123 (1991).
[17] R. Müller, T. Schweirer, P. Bohec, R.O. Suzuki, and I. J. Gaukler, Physica **C 203,** 299 (1992).
[18] T. G. Holesinger, D. J. Miller, L. S. Chumbley, M. J. Kramer, and K. W. Dennis, Physica **C 202,** 109 (1992).
[19] P. Majewski, B. Freilinger, B. Hettich, T. Popp, and K. Schulze, in: Hight-Temp. Supercond. Proc. ICMC 90 Top.-Conf. Mater. Aspects High-Temp. Supercond., Vol. 1, p. 393–398 (1991), (H. C. Freyhardt, R. Fluekiger, and M. Peuckert, eds.), Oberursel, FRG, as taken from Chemical Abstracts **119** (8): 81210u (1991) and from [18].